# Identifying zeolite topologies for storage and release of hydrogen

Martin-Calvo, A.; Gutiérrez-Sevillano, J.J.; Matito-Martos, I.; Vlugt, T. J.H.; Calero, S.

**DOI**
10.1021/acs.jpcc.8b02263

**Publication date**
2018

**Document Version**
Accepted author manuscript

**Published in**
Journal of Physical Chemistry C

# Identifying Zeolite Topologies for Storage and Release of Hydrogen

A. Martin-Calvo [b], J. J. Gutiérrez-Sevillano *[c], I. Matito-Martos [a], T. J. H. Vlugt [d], and S. Calero *[a]

**Abstract:** We present a molecular simulation study on the most suitable zeolite topologies for hydrogen adsorption and storage. We combine saturation capacities, pore size distributions, preferential adsorption sites and curves of heat of adsorption of hydrogen as function of temperature (we call them HoA-curve) to identify the optimal zeolites for storage and release of hydrogen. Then we analyze the relation between the shape of the HoA-curve and the topology of the materials. We also evaluate the influence of incorporating Feynman-Hibbs effect on the adsorption behavior. We can stablish different shapes on the HoA-curve depending on the uniformity or not of the pores of the zeolites. Parabola-like curves are observed in structures with one or similarly sized pores, while deviations from the parabola are found at low temperature for structures combining large and small pores. The Feynman-Hibbs quantum correction reduces the adsorption capacity of the materials affecting not only the saturation capacity but also the shape of the isotherms. From our results the zeolites studied in this work can be considered potential candidates for the storage and release of hydrogen.

## Introduction

Optimization of porous materials to improve their separation, storage, and catalytic properties is an on-going challenge faced by many scientists.[1] Energy storage technologies are based on emerging materials with the aim of lowering costs while increasing simultaneously the storage/release efficiency.[2] One of the objectives set by the U.S. Department of energy (DOE) for 2017 is the development of automotive hydrogen storage systems achieving 5.5wt.% hydrogen in gravimetric capacity and 40 g hydrogen/L in volumetric capacity at mild conditions and low cost.[3] These criteria cannot be met by any available material yet, and it is in this contest where simulation studies are suggesting strategies to identify porous materials optimal enough to reach the gravimetric target.[4] One of the approaches to reach this goal is to store molecules in porous media based on physisorption mechanisms. Porous materials share the common features of uniform and regular pores that can be described using parameters such as size, shape and volume of the pore, occupiable and accessible volume, surface area, size of the windows, or channel dimensionality among others. Zeolites are the most important family in microporous materials, conventionally are based on $TO_4$ tetrahedra where the T atom is typically Si or Al. The tetrahedra form three dimensional frameworks with pores of molecular dimensions. Current zeolites are described in the Database of Zeolite Structures[5] and up to now the number of entries have risen to 232. Each topology is assigned a three-capital letter code in alphabetical order that describes the network of tetrahedrally coordinated framework atoms, independently of the composition, the distribution of the T atoms, or the dimensions and symmetry of the unit cell.

The adsorption of hydrogen in zeolites involves the interaction of the molecule with the internal surface of their pores. This physisorption is governed by van der Waals interactions between hydrogen and the zeolite, including low interaction potentials and heats of adsorption. Unfortunately, weak physisorption implies low values of temperature to achieve reasonable loadings.

At room temperature and atmospheric pressure, none of the current zeolites has a storage capacity to meet the target value, so storage in these structures needs to be cryogenic and/or pressure systems. However, hydrogen storage under these conditions is directly related to increasing safety risks and costly processes.[6] Therefore, moderate working conditions would be optimal to validate the viability of the materials for this purpose. For hydrogen, a typical temperature of 77 K, i.e. temperature of liquid nitrogen and pressures of at least 2 MPa and up to 10 MPa would be ideal.[7]

The first studies on zeolites for hydrogen storage were focused on structures with sodalite cages[8] but the storage capacities of these structures are very low at room temperature, increasing at 77 K up to 1.5wt% in the case of FAU.[9] This capacity still falls short of relevant values. The highest storage capacity (2.19 wt%) on a FAU zeolite was found on a Ca-exchanged material.[10] Note that the storage capacity of this zeolite increases with the number of cations inside the structure. At cryogenic temperatures CHA exhibits hydrogen capacity of 1.28 wt%.[11] Zeolite ITT has a pore volume of 0.37 cm3/g. When the structure is filled with hydrogen at liquid hydrogen density, the storage capacity reaches 2.5 wt%.[12] To the best of our

[a] Prof. S. Calero, I. Matito-Martos
Department of Physical, Chemical, and Natural Systems, University Pablo de Olavide
Ctra. de Utrera, km. 1, 41013 Seville, Spain
E-mail: scalero@upo.es
[b] Dr. A. Martin-Calvo
Department of Chemical Engineering, Vrije Universiteit Brussel
Pleinlaan 2, 1050, Brussels, Belgium
[c] Dr. J. J. Gutierrez-Sevillano
Center for Molecular Modeling, Ghent University
Technologiepark 903, B9000, Ghent, Belgium
E-mail: juanjose.gutierrezsevillano@ugent.be
[d] Prof. T. J. H. Vlugt
Engineering Thermodynamics, Process & Energy Department, Delft University of Technology Center for Molecular Modeling
Leeghwaterstraat

Supporting information for this article is given via a link at the end of the document

knowledge this is the zeolite with the highest hydrogen capacity reported to date.

Based on the above-mentioned works and considering that our study is performed at temperatures between 25 and 350 K and pressures up to 100 MPa, we are focusing on pure silica zeolites with the goal of finding structures with storage capacities above 2.5 wt% at 77 K and above 4 wt% at 25 K. We are perfectly aware that these capacities are still well below practical targets however, they are significant and deserve further study, especially if we take into account that zeolites are advantageous over other sorbent materials for their low cost and high thermal stability. The use of pure silica structures allows to stablish a lower bound of the maximum storage capacity of the materials. Adding cations would lead to higher storage capacities nevertheless, a quantitative study of the uptake variations as a function of the type and number of cations would be object of a completely different work.

Experimental and simulation studies have demonstrated that hydrogen adsorption capacity in zeolites depends on the framework topology, composition, micropore volume, specific surface area, and channel diameter, as well as the type of non-framework cations.[8, 13] Adsorption capacity is maximized in structures that exhibit a proper balance between these factors.[11, 14] From these studies it is clear that the idea of designing novel zeolites as materials for the storage and release of hydrogen has not yet been discarded. A given material is capable to store hydrogen only if the heat of adsorption of this molecule is strong enough to adsorb a large amount of gas at the charging pressure but weak enough to release most of this gas at the discharge pressure. It has also been proven that the amount of hydrogen adsorbed in the structure correlates at low loading with the heat of adsorption, at medium loading with the surface area, and at high loading with the free volume.[15] Our aim is to analyze the performance of all available zeolites and to use this knowledge for the selection of the best ones for hydrogen storage and release as well as the optimal conditions at which these processes should take place. We base the analysis on relations between saturation capacities, isosteric heats of adsorption, pore size distributions, and preferential adsorption sites, with the final goal of interpreting the curves of heats of adsorption in terms of hydrogen and storage release.

## Results and Discussion

To get an overall impression of the adsorption capacity of the 219 zeolites, we computed the weight percentage of hydrogen in gravimetric capacity at moderate (77 K and 1 MPa) and extreme (25 K and 100 MPa) working conditions. We chose these conditions in order to compare with the storage capacities of FAU, CHA, and ITT reported in the literature [9, 11-12]. Figure 1 shows the weight percentage of hydrogen as a function of the zeolite surface area at a) 77 K and 1 MPa, and b) at 25 K and 100 MPa. Contrary to the reported values for ITT (2.5 wt%), our simulations show that the storage capacity of hydrogen for this zeolite is 1.5 wt%. We found also structures such as IRR, PUN, AFY, JST, OSO, and JSR, with higher saturation capacity and larger surface area that ITT, but still below 2.5 wt%. Simulations at moderate conditions (77 K and 1 MPa), point out only four zeolites which storage capacity of hydrogen is above 2.5 wt%: NPT (2.83 wt%), RWY (2.66 wt%), OBW (2.6 wt%), and BOZ (2.53 wt%). At extreme conditions (25 K and 100 MPa) the storage capacity of these zeolites is clearly larger than 2.5 wt%. In fact, we found a set of zeolites with saturation capacity above 4 wt% of hydrogen, one of them with more than 7 wt% of hydrogen: RWY (7.18 wt%), IRR (4.53 wt%), OBW (4.48 wt%), NPT (4.24 wt%), JSR (4.08 wt%) and BOZ (3.86 wt%). These adsorption capacities were somehow in contradiction with the theoretical work reported by Vitillo and coworkers, in which they concluded that the zeolite capacities are intrinsically limited to a maximum of 2.86 wt% due to their geometrical contains. These values were obtained for FAU and RHO, computing the maximal capacities for 12 zeolite topologies at 0 K and zero pressure[13a]. The capacities that we obtained for FAU and RHO were 1.85 wt% and 2.08 wt% at moderate working conditions and 3.45 wt% and 3 wt% at extreme conditions. All values are collected in Table S1 of the Electronic Supporting Information (ESI).

The core of our study will focus on the 6 zeolites with the highest storage capacity, comparing them with ITT zeolite. From a topological point of view, these zeolites do not share any specific feature to explain their better performance. Some of them have certain similarities, but in general they are quite different. To gain insights on the differences between zeolites, we compute the heat of adsorption of hydrogen on each structure in a wide

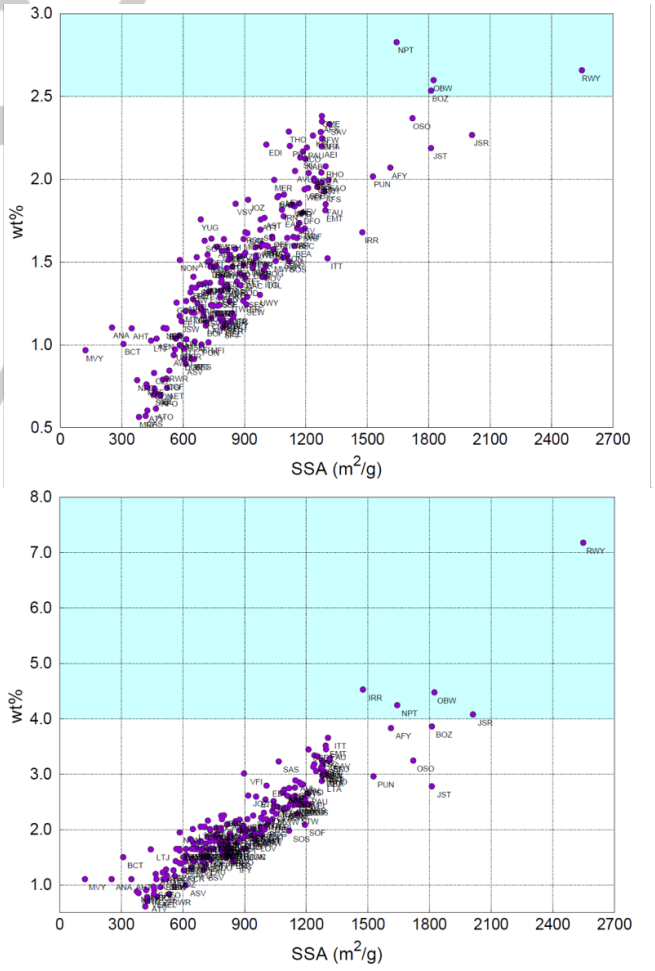


**Figure 1.** Hydrogen weight percentage as a function of surface area at 77 K and 1 MPa (top) and 25 K and 100 MPa (bottom). Light blue indicates the region where hydrogen weight percentage of the structures is above the stablished benchmarks of 2.5 (top) and 4 (bottom).

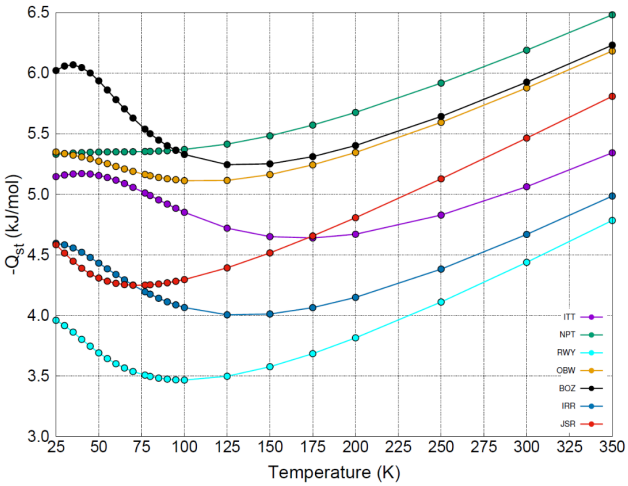


**Figure 2.** HoA-curves of ITT, NPT, RWY, OBW, BOZ, IRR, and JSR.

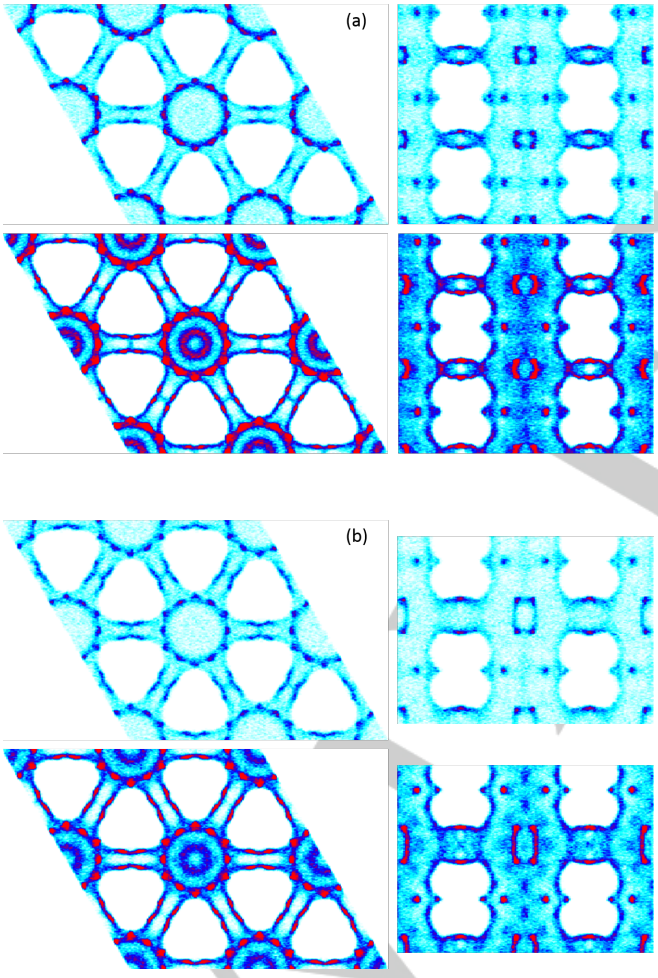


**Figure 3.** *XY* (left) and *YZ* (right) views of the Average Density Profiles of hydrogen at 77 K and 1 MPa (top) and 100 MPa (bottom) in ITT (a) and IRR (b). The color gradation indicates the occupational density (white-cyan-blue-red).

range of temperature. Plotting the heat of adsorption as a function of temperature we obtain what we name the heat of adsorption curve (HoA-curve). Then, we base the analysis on a combination of these HoA-curves, the topology of the structures, and the adsorption isotherms. Figure 2 shows the HoA-curves of ITT, RWY, BOZ, JSR, NPT, OBW, and IRR. The heat of adsorption obtained for ITT is almost independent of temperature (about 5 kJ/mol). This zeolite consists of a 3D channel system with large straight pores with circular openings of 18-rings along the c axis interconnected by a bidirectional system of 10-ring channels. The pore size distribution of the structure (Figure S2 of the ESI) shows two picks at 5 and 12 Å approx. The larger peak corresponds to the wide longitudinal channels while the smaller one to the narrow channels intersecting with the main channels. The molecule of hydrogen commensurate well in the channels of 5 Å leading to constant values of the heat of adsorption in a large range of temperature. The largest channels are filled with increasing pressure and consequently with loading as shown in Figure 3.

The quantum effect mimicked with a Feynman-Hibbs correction, becomes important for adsorption at low values of temperature. As can be observed in Figure S1 from the ESI, when the Feynman-Hibbs corrections is incorporated to the Lennard-Jones potential, the minimum of the potential shifts to longer distances. For host-guest interactions, this implies a reduction of the available space for adsorption. In the case of guest-guest interactions, the shift means that the adsorbed molecules are more separated. The combination of both factors leads to a reduction of the maximum loading of a structure. For ITT, this effect is significant at 25 K, but is almost inexistent at higher temperatures. At 25 K, the molecules of hydrogen enter the structure at 10-3 Pa, i.e. five orders of magnitude lower than at 50 K, as a result of a combination of the effective potential and the particular pore size distribution of the structure (Figure 4). At temperature higher than 50 K the quantum effect of hydrogen is lower and almost negligible for temperatures larger than 100 K. Among the 6 selected zeolites, only IRR has a similar topology than ITT but the pore size distribution shows channels and cavities wider than ITT (Figure S3 for the ESI). This explains on the one hand the lower values of heat of adsorption at the same temperature, and on the other hand the largest storage capacity and saturation values obtained for this structure. Figure 3 shows that the density profiles obtained for the two zeolites are rather similar, but for ITT the intersections between small big and small channels are preferential adsorption sites whereas for IRR this preferential adsorption site disappears (since the small channels are wider than these in ITT). These differences on the preferential adsorption sites are translated into different adsorption isotherms in both zeolites. As can be observed in Figure 4, hydrogen adsorption begins at lower values of pressure in ITT while the saturation values are larger in IRR. Nevertheless, the Feynman-Hibbs effect still stands at 25 K (adsorption of hydrogen at this temperature starts at 10-2 Pa, two orders of magnitude lower than at 50 K) and the effect at saturation is also appreciable for this zeolite (decrease of saturation loadings compared to these at higher temperature). The heats of adsorption of JSR at low values of temperature are like the obtained for IRR since both structures show a peak at about 6 Å in the Pore Size Distribution, corresponding to the small channels in IRR and the irregular cavities of JSR (Figure

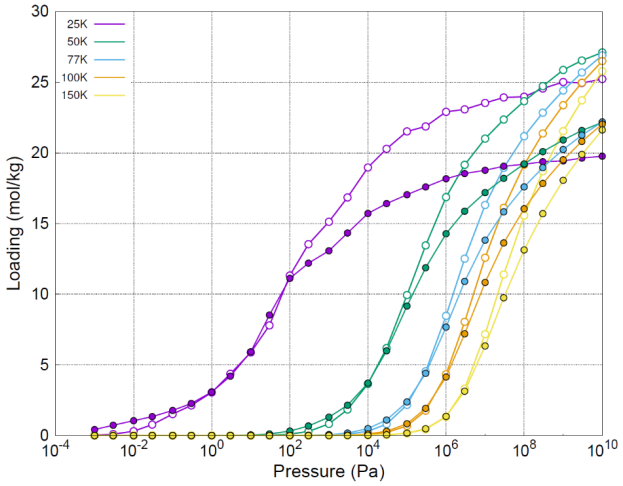


**Figure 4.** Adsorption isotherms of hydrogen in ITT (full symbols) and IRR (empty symbols).

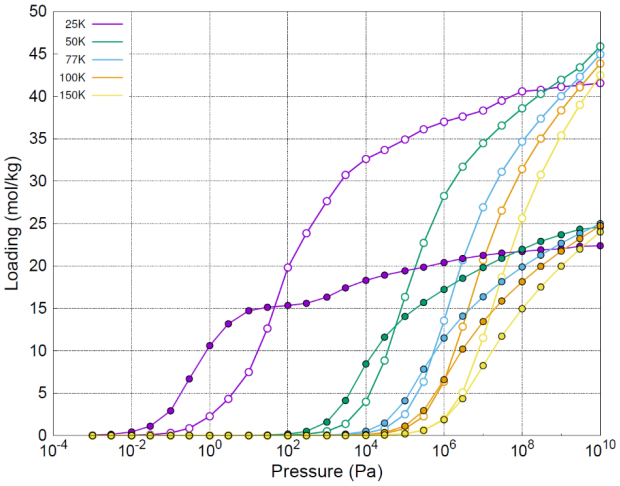


**Figure 5.** Adsorption isotherms of hydrogen in JSR (full symbols) and RWY (empty symbols).

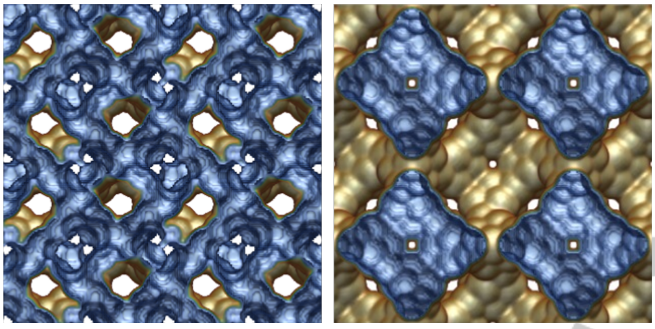

**Figure 6.** Energy Grid Profile of JSR (left) and RWY (right). All views are identical. Brown and blue colors represent the accessible and inaccessible surface, respectively.

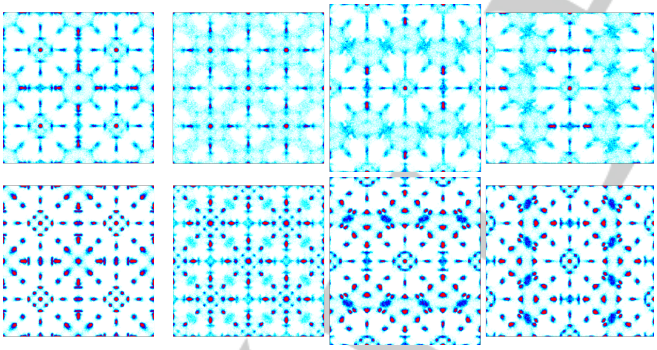

**Figure 7.** Average Density Profiles of hydrogen at 77 K and 1 MPa (top) and 100 MPa (bottom) in NPT (left, all views are identical) and OBW (right, XY, YZ, and ZX views). The color gradation indicates the occupational density (white-cyan-blue-red).

S4 of the ESI). Contrary to IRR, JSR is highly isotropic exhibiting only one type of cavities or channels (Figure S5 of the ESI). This fact together with the lack of preferential adsorption sites explain the linear behavior of the heats of adsorption for increasing temperature. It is remarkable that, despite its isotropy, JSR and IRR share cavities with the same minimal length size and this can be responsible of the similar influence of the Feynman-Hibbs contribution at 25 K in the saturation regime (Figure 5).

This effect is much lower for RWY, also isotropic, but formed by more homogeneous cavities than JSR (Figure 6). The pore size distribution of RWY shows one single pick at 14 Å that explains the low values of the heat of adsorption as well as the large values in saturation capacity (Figure S6 of the ESI).

The last isotropic zeolite identified in this work as potential structure for hydrogen storage is NPT. The pore size distribution of this structure indicates two cavities with peaks at about 5 and 9.5 Å (Figure S7 of the ESI). This structure is formed by 3- , 4-, and 8-membered rings leading to a 3D system of channels. Big cavities are indirectly connected to each other through narrowness that communicate with smaller cavities. These small cavities (formed by 8-membered rings) form an intersected system of channels (Figure S8 of the ESI). The particular topology of this structure provides preferential adsorption sites at the constrictions of the pores that are indicated in the pore side distribution by a wide peak at about 3.5 Å (Figure 7). This narrowness also explains the relatively high values of heat of adsorption at low temperature that remain constant up to 100 K. The preferential adsorption sites at the constrictions of the pore are also evidenced in the adsorption isotherm at 25 K (Figure 8). It is also interesting to note that the Feynman-Hibbs contribution does not affect saturation values for this zeolite. A similar behavior is found on OBW. This zeolite contains 3-, 4-, 8-, and 10-membered rings on its structure, and a 3D system that reminds to this of NPT. Two main cavities are observed of 5.5 and 8.5 Å approx. (Figure S9). In a similar way as occurred in NPT, big cavities are connected via constrictions to the smaller cavities (Figure S10 of the ESI). However, the complexity of this topology is enhanced by its lack of isotropy. The particularities of this framework also reveal strong preferential adsorption sites that can be translated into high heats of adsorption, nevertheless, contrary to what we observed on NPT, they are not constant at low temperature. Compared to NPT the effect of the Feynman-Hibbs correction at 25 K in this zeolite is more significant at saturation values (Figure 9). However, there is a remarkable effect in both zeolites at intermediate values of pressure (between $10^{-1}$ and $10^{5}$ Pa) where not only the adsorption capacity but also the shape of the isotherm is modified. This effect is more evident in OBW than in NPT.

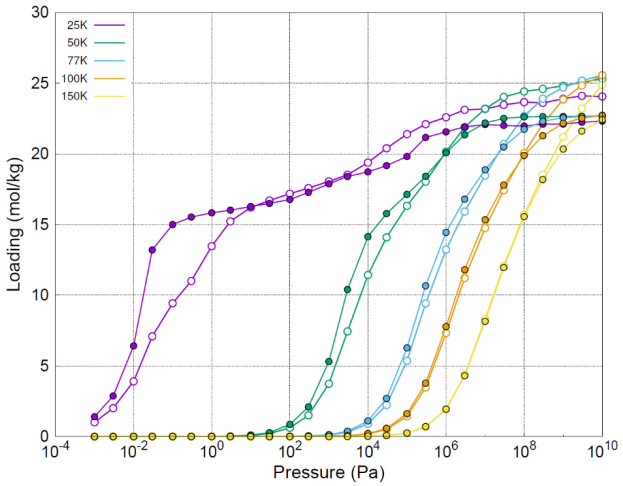


**Figure 8.** Adsorption isotherms of hydrogen in NPT (full symbols) and OBW (empty symbols).

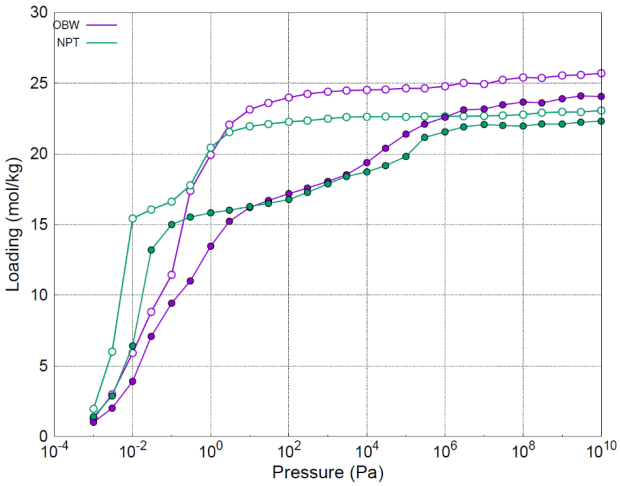


**Figure 9.** Adsorption isotherms of hydrogen in NPT (green) and OBW (purple) at 25 K with and without Feynman-Hibbs quantum correction (full and empty symbols, respectively).

We identify BOZ as the zeolite with the highest heats of adsorption. This is attributed to a combination of a) the presence of four peaks in the pore size distribution (Figure S11 of the ESI) and b) the anisotropic character of the structure. This zeolite has a 3D network of channels formed by 3-, 4-, 6-, 8-, and 10-membered rings. This leads to four types of cavity of 3, 4.5, 6.5, and 8 Å. According to the topology, different channels are identified, being their cranny shape and narrow connections the responsible of the presence of preferential adsorption sites for hydrogen, and therefore of the high heats of adsorption (Figure 10). Similarly to what we observed for ITT, the Feynman-Hibbs correction has an impact on the adsorption capacity of this zeolite, with strong effect at 25 K (Figure S12 of the ESI).

Based on our simulations we can stablish relations between the topology of the structures (PSDs and channel system) and the HoA-curves (Figure 2). The molecular model used for hydrogen is slightly larger than its kinetic diameter (2.89 Å). Therefore, structures with the smallest pore of about 3 Å in diameter do not show any specific behavior (hydrogen molecules do not enter these pores). However, sorting the zeolites based on their next smallest pore (from smaller to larger pore size), they follow the reverse order as the heat of adsorption of the structures at the lowest temperature (25 K). As expected smaller pores result on higher heat of adsorption. Nevertheless, the shape of the HoA-curve varies depending on the type and size of the remaining pores of the frameworks. Structures with just one type of pore (RWY) or with more than one but similar in size (JSR) show a parabola-like shape on the HoA-curve, being the minimum heat of adsorption shifted to lower temperatures on structures with smaller pores (from 100 to 75 K on RWY and JSR with pores of about 13 and 6-7 Å, respectively). The shape of the HoA-curve can deviate from the parabola in the 0 K range, when different pore sizes are combined in the structure. Similar shapes are found for ITT and IRR, both structures combining small pores of about 5 Å with large pores of 12.5 and 12-13.5 Å, respectively. The small pore is responsible of the small kink that can be observed at temperatures between 30 and 50 K in ITT and at 30 K in IRR (this kink is less remarkable in IRR since its small pore is slightly larger than this of ITT). Above 50 K, the general V-shape remains, with the lowest values of heat of adsorption on

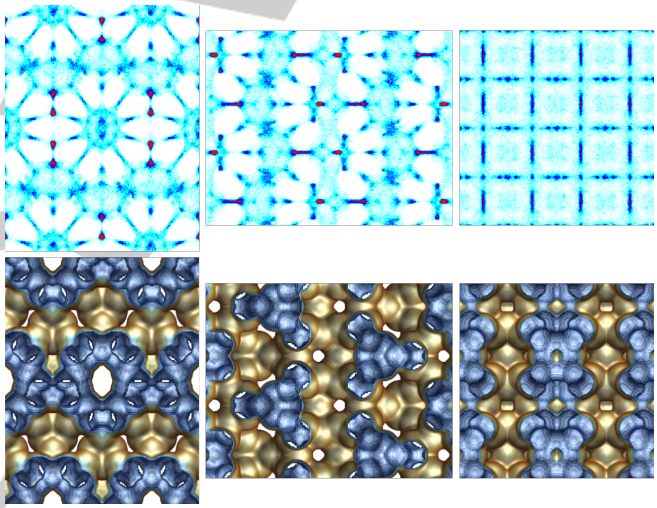

**Figure 10.** From left to right, XY, YZ, and ZX views of the average density profiles of hydrogen at 1MPa (top) and energy grid profile (bottom) of BOZ. Brown and blue colors represent the accessible and inaccessible surface, respectively. The color gradation indicates the occupational density (white-cyan-blue-red).

the structure with the largest pores. IRR with pores of 12 Å shows its minimum at 125 K, while this value is shifted to 175 K on ITT with slightly larger pore (12.5 Å). When the structures contain a combination of pores similar in size (NPT and OBW), the kink observed on the HoA-curves are less noticeable. The two structures contain small pores of about 5 Å and large pores of 8.5 Å (OBW) and 9.5 Å (NPT). With these PSDs, one would expect similar behavior than for ITT and IRR. However, this is just partially true for OBW, with less effect due to the smaller size of the big pore of this structure. On the contrary, the already mentioned presence of constrictions together with the isotropic nature of NPT make the HoA-curve not a parabola-like function, becoming flat up to 100 K. Finally, the combination of more than 2 types of pore sizes (BOZ) shows the strongest deviations of the HoA-curve, being the structure with the largest differences between maximum (6.1 kJ/mol at 35 K) and minimum (5.2

kJ/mol at 125 K) heat of adsorption. Above 200 K all HoA-curves follow the same trend since the high thermal contribution overcomes topological factors on the calculation of the heat of adsorption. In this regard, we observe that the HoA-curves can provide information about the topology of the materials, but heats of adsorption must be computed below 200K.

## Conclusions

In this work, we screened the hydrogen adsorption capacity of the 219 zeolites from the IZA Database by computing the weight percentage of hydrogen at moderate (77 K and 1 MPa) and extreme (25 K and 100 MPa) working conditions. For a target capacity of 4 wt% at 25 K, we found a set of 6 zeolites with saturation capacity above this value (RWY, IRR, OBW, NPT, JSR, and BOZ), showing RWY the maximum capacity with 7wt%. We computed adsorption isotherms, pore size distributions, preferential adsorption sites, and heat of adsorption of hydrogen at different temperatures on each structure, as well as on ITT, since this is considered the zeolite with the highest hydrogen capacity reported to date. We established relations between the HoA-curves obtained by plotting the heat of adsorption versus temperature and the topology of the structures. (1) Structures with one type of pore or with more than one but similar in size show a parabola-like curve. (2) Structures with small and large pores show HoA-curves with a kink at the lowest temperatures. This kink depends on the size of the smallest pore. Regarding the computed isotherms, the use of Feynman-Hibbs quantum correction leads to a decrease of the adsorption that not only affects the saturation capacity but also the shape of the isotherm. Based on our results we consider that the mentioned zeolites can be potential candidates for the storage and release of hydrogen.

## Simulation Section

Our molecular simulations for energy storage materials are enhanced by constant update in calculation methods,[16] force fields,[17] and optimized models.[18] In this study, we face the advantages and disadvantages of simulating one of the smallest molecules that can be adsorbed in a porous material. The small size of the molecule of hydrogen and the relatively large rigidity of most zeolites allow to neglect flexibility. However, the mere combination of Lennard-Jones and Coulomb potentials could be insufficient to describe the interactions between such a small molecule and the porous material, requiring specific interactions in order to reproduce experimental adsorption.[18a, 19] At the cryogenic temperatures of our study, the quantum behavior of hydrogen is non-negligible in the nanoscale confinement of zeolite pores and other nanostructured materials.[6a, 18a, 20] Therefore, we use for hydrogen the model proposed by Deeg *et al.*[18a] with a single uncharged Lennard-Jones center that incorporates quantum effects through a Feynman-Hibbs effective interaction potential (Figure S1). This model was validated with experimental adsorption of hydrogen in pure silica LTA (ITQ-29) and MFI at 25, 77, 90, and 120 K. The structures of the zeolites were taken from the Database of Zeolite Structures.[5] Among them, 13 topologies (CHI, CLO, EWT, IFU, IRY, ITN, ITV, LIT, PAR, RON, SSO, SVR, and WEN) were discarded as the coordination of the silicon atoms is not tetrahedral. The remaining 219 topologies were modeled as rigid frameworks in their pure silica form using previosuly validated force field parameters.[21]

Saturation capacities and absolute adsorption isotherms were calculated by Monte Carlo simulations in the Grand-Canonical ensemble, and for heats of adsorption (HoA) under diluted conditions we used the Widom test particle method.[22] Surface area (SSA) and Pore Size Distribution (PSD) of the materials are computed geometrically.[23] A cutoff of 12 Å is applied to the Lennard-Jones and Feynman-Hibbs potentials. Rotation, translation and reinsertion are the main movements applied to the molecules. No partial blockage of the structures is applied, since all their cavities are accessible for the molecule of hydrogen. Simulations were performed with the molecular simulation software RASPA.[24]

## Acknowledgements

This work has been supported by the Spanish “Ministerio de Economia y Competitividad” (CTQ2016-80206-P) and by the “Junta de Andalucia” (P12-FQM-1851). JJ.G-S thanks the Research Council of Ghent University for his BOF-postdoctoral fellowship. I.M-M acknowledges the Spanish “Ministerio de Educación Cultura y Deporte” for his predoctoral fellowship (FPU13/00281). TJH.V is grateful to NWO-CW for his VICI grant.

**Keywords:** hydrogen • adsorption • topology • zeolite • simulation

[1] a) F. Akhtar, L. Andersson, S. Ogunwumi, N. Hedin, L. Bergstrom, *Journal of the European Ceramic Society* **2014**, *34*, 1643-1666; b) N. Z. Logar, V. Kaucic, *Acta Chimica Slovenica* **2006**, *53*, 117-135; c) M. I. Nandasiri, S. R. Jambovane, B. P. McGrail, H. T. Schaef, S. K. Nune, *Coordination Chemistry Reviews* **2016**, *311*, 38-52; d) G. Sneddon, A. Greenaway, H. H. P. Yiu, *Advanced Energy Materials* **2014**, *4*; e) A. W. Thornton, D. A. Winkler, M. S. Liu, M. Haranczyk, D. F. Kennedy, *Rsc Advances* **2015**, *5*, 44361-44370; f) C. D. Wu, M. Zhao, *Advanced Materials* **2017**, *29*; g) Z. Xie, Y. S. Li, L. Chen, D. L. Jiang, *Acta Polymerica Sinica* **2016**, 1621-1634.

[2] a) H. Bin Wu, X. W. Lou, *Science Advances* **2017**, *3*; b) K. Fu, Y. G. Yao, J. Q. Dai, L. B. Hu, *Advanced Materials* **2017**, *29*; c) Kenry, C. T. Lim, *Progress in Polymer Science* **2017**, *70*, 1-17; d) H. L. Wang, Q. L. Zhu, R. Q. Zou, Q. Xu, *Chem* **2017**, *2*, 52-80; e) W. Xia, A. Mahmood, R. Q. Zou, Q. Xu, *Energy & Environmental Science* **2015**, *8*, 1837-1866; f) J. W. Zhou, B. Wang, *Chemical Society Reviews* **2017**, *46*, 6927-6945.

[3] US Department of Energy, Office of Energy Efficiency & Renewable Energy, *Fuel Cell Technologies Program Multi-Year Research, Development and Demonstration Plan*: https://energy.gov/eere/fuelcells/downloads/fuel-cell-technologies-office-multi-year-research-development-and-22

[4] a) Z. X. Yang, Y. D. Xia, R. Mokaya, *Journal of the American Chemical Society* **2007**, *129*, 1673-1679; b) S. S. Han, W. A. Goddard, *Journal of the American Chemical Society* **2007**, *129*, 8422-+; c) R. B. Getman, J. H. Miller, K. Wang, R. Q. Snurr, *Journal of Physical Chemistry C* **2011**, *115*, 2066-2075; d) J. Jiang, R. Babarao, Z. Hu, *Chemical Society Reviews* **2011**, *40*, 3599-3612; e) J. R. Li, R. J. Kuppler, H. C. Zhou, *Chemical Society Reviews* **2009**, *38*, 1477-1504; f) Y. J. Colon, R. Q. Snurr, *Chemical Society Reviews* **2014**, *43*, 5735-5749.

[5] Ch. Baerlocher, L. B. McCusker, *Database of Zeolite Structures*: http://www.iza-structure.org/databases/

[6] a) S. K. Bhatia, A. L. Myers, *Langmuir* **2006**, *22*, 1688-1700; b) S. Yunes, P. Wommack, M. Still, J. Kenvin, J. Exley, *Applied Catalysis a-General* **2014**, *474*, 250-256.

[7] U. Eberle, M. Felderhoff, F. Schuth, *Angewandte Chemie-International Edition* **2009**, *48*, 6608-6630.

[8] J. Weitkamp, M. Fritz, S. Ernst, *International Journal of Hydrogen Energy* **1995**, *20*, 967-970.

[9] S. H. Jhung, J. W. Yoon, S. Lee, J. S. Chang, *Chemistry-a European Journal* **2007**, *13*, 6502-6507.

[10] H. W. Langmi, D. Book, A. Walton, S. R. Johnson, M. M. Al-Mamouri, J. D. Speight, P. P. Edwards, I. R. Harris, P. A. Anderson, *Journal of Alloys and Compounds* **2005**, *404*, 637-642.

[11] L. Regli, A. Zecchina, J. G. Vitillo, D. Cocina, G. Spoto, C. Lamberti, K. P. Lillerud, U. Olsbye, S. Bordiga, *Physical Chemistry Chemical Physics* **2005**, *7*, 3197-3203.

[12] A. Corma, M. J. Diaz-Cabanas, J. L. Jorda, C. Martinez, M. Moliner, *Nature* **2006**, *443*, 842-845.

[13] a) J. G. Vitillo, G. Ricchiardi, G. Spoto, A. Zecchina, *Physical Chemistry Chemical Physics* **2005**, *7*, 3948-3954; b) H. W. Langmi, A. Walton, M. M. Al-Mamouri, S. R. Johnson, D. Book, J. D. Speight, P. P. Edwards, I. Gameson, P. A. Anderson, I. R. Harris, *Journal of Alloys and Compounds* **2003**, *356*, 710-715; c) A. A. G. Blanco, A. F. Vallone, A. Gil, K. Sapag, *International Journal of Hydrogen Energy* **2012**, *37*, 14870-14880; d) C. O. Arean, D. Nachtigallova, P. Nachtigall, E. Garrone, M. R. Delgado, *Physical Chemistry Chemical Physics* **2007**, *9*, 1421-1436; e) M. Rahmati, H. Modarress, *Applied Surface Science* **2009**, *255*, 4773-4778; f) A. W. C. van den Berg, S. T. Bromley, J. C. Wojdel, J. C. Jansen, *Microporous and Mesoporous Materials* **2006**, *87*, 235-242.

[14] a) A. Zecchina, S. Bordiga, J. G. Vitillo, G. Ricchiardi, C. Lamberti, G. Spoto, M. Bjorgen, K. P. Lillerud, *Journal of the American Chemical Society* **2005**, *127*, 6361-6366; b) M. Bastos-Neto, C. Patzschke, M. Lange, J. Mollmer, A. Moller, S. Fichtner, C. Schrage, D. Lassig, J. Lincke, R. Staudt, H. Krautscheid, R. Glaser, *Energy & Environmental Science* **2012**, *5*, 8294-8303; c) J. X. Dong, X. Y. Wang, H. Xu, Q. Zhao, J. P. Li, *International Journal of Hydrogen Energy* **2007**, *32*, 4998-5004; d) M. G. Nijkamp, J. Raaymakers, A. J. van Dillen, K. P. de Jong, *Applied Physics a-Materials Science & Processing* **2001**, *72*, 619-623.

[15] a) H. Frost, T. Duren, R. Q. Snurr, *Journal of Physical Chemistry B* **2006**, *110*, 9565-9570; b) H. Frost, R. Q. Snurr, *Journal of Physical Chemistry C* **2007**, *111*, 18794-18803.

[16] A. Poursaeidesfahani, A. Torres-Knoop, M. Rigutto, N. Nair, D. Dubbeldam, T. J. H. Vlugt, *Journal of Physical Chemistry C* **2016**, *120*, 1727-1738.

[17] A. Martin-Calvo, J. J. Gutierrez-Sevillano, J. B. Parra, C. O. Ania, S. Calero, *Physical Chemistry Chemical Physics* **2015**, *17*, 24048-24055.

[18] a) K. S. Deeg, J. J. Gutierrez-Sevillano, R. Bueno-Perez, J. B. Parra, C. O. Ania, M. Doblare, S. Calero, *Journal of Physical Chemistry C* **2013**, *117*, 14374-14380; b) P. Gomez-Alvarez, S. Hamad, M. Haranczyk, A. R. Ruiz-Salvador, S. Calero, *Dalton Transactions* **2016**, *45*, 216-225.

[19] a) T. Pham, K. A. Forrest, P. Nugent, Y. Belmabkhout, R. Luebke, M. Eddaoudi, M. J. Zaworotko, B. Space, *Journal of Physical Chemistry C* **2013**, *117*, 9340-9354; b) R. B. Getman, Y.-S. Bae, C. E. Wilmer, R. Q. Snurr, *Chemical Reviews* **2012**, *112*, 703-723.

[20] A. V. A. Kumar, H. Jobic, S. K. Bhatia, *Journal of Physical Chemistry B* **2006**, *110*, 16666-16671.

[21] A. Garcia-Sanchez, C. O. Ania, J. B. Parra, D. Dubbeldam, T. J. H. Vlugt, R. Krishna, S. Calero, *Journal of Physical Chemistry C* **2009**, *113*, 8814-8820.

[22] B. Widom, *Journal of Chemical Physics* **1963**, *39*, 2808-&.

[23] a) L. D. Gelb, K. E. Gubbins, *Langmuir* **1999**, *15*, 305-308; b) L. Sarkisov, A. Harrison, *Molecular Simulation* **2011**, *37*, 1248-1257.

[24] a) D. Dubbeldam, S. Calero, D. E. Ellis, R. Q. Snurr, *Molecular Simulation* **2016**, *42*, 81-101; b) D. Dubbeldam, A. Torres-Knoop, K. S. Walton, *Molecular Simulation* **2013**, *39*, 1253-1292.

**Entry for the Table of Contents**

Layout 1:

## FULL PAPER

Relationship between topology of the material and the shape of the HoA-curve, from which optimal conditions for hydrogen adsorption/release can be obtained.

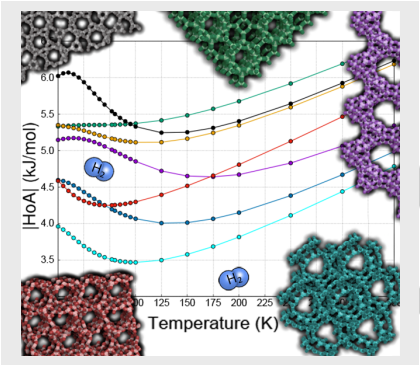


*A. Martin-Calvo, J. J. Gutiérrez-Sevillano*, I. Matito-Martos, T. J. H. Vlugt, S. Calero**

***Page No. – Page No.***

**Identifying Zeolite Topologies for Storage and Release of Hydrogen**